Włodzimierz BĘDKOWSKI*, Bienvenu KENMEUGNE**,
Ewald MACHA*, Jean-Louis ROBERT**

On the Prediction of the Fracture Plane Orientation in Multiaxial Fatigue

* Department of Mechanics and Machine Design - Technical University of Opole, Opole, Poland
** INSA de Lyon - Laboratory of Solid Mechanics - Villeurbanne CEDEX, France

Keywords: biaxial fatigue, random loadings, critical fracture plane, fracture plane direction, variance method, damage indicator method, fatigue criteria

ABSTRACT: Two methods that allow to predict the fracture plane orientation are presented and compared in this paper. The first one is a statistical approach which is based on the variance of an equivalent stress. It is assumed that the fracture plane is the one where the variance of a linear combination of the shear and normal stresses acting on this plane is maximum. The second one uses the so-called damage indicator of a multiaxial fatigue criterion, which is based on the research of the critical plane. The formulation of the criterion involves shear and normal stress amplitudes and mean normal stress. The fracture plane is the critical plane, it is to say the one where the damage indicator is the highest. A comparison of the two methods against experimental results is made for multiaxial cyclic and random stress states.

Introduction

Most mechanical components or structures are nowadays designed as fatigue-prone components. The industrial purpose is to improve their service safety to avoid mechanical failures and to lower the cost of maintenance. This is why many industrial engineers or academical researchers have worked during the last decades both on experiments and theoretical fatigue models to improve the understanding and modelling of the fatigue behaviour of materials. The major objective in fatigue is to assess the fatigue life of the component submitted to variable loading. This induces various states of stress in any point of the structure. The fatigue assessment is realized everywhere in order to find out the critical area of the component. An important point of fatigue behaviour models is the determination of the crack initiation plane because it is required to calculate the fatigue life.

The so-called critical plane is the one where the crack initiates and will develop. The material life can then be established through the normal and shear stresses that are applied on it.

The aim of this paper is to present and discuss two different methods for determining the crack initiation plane. One is a statistical approach that is developed by the Departement of Mechanics and Machine Design of the Technical University of Opole (Poland) (1). The second one is a stress-based approach that is proposed by the Laboratory of Solid Mechanics of INSA Lyon (France) (2)

The Polish point of view is the so-called variance method. An equivalent stress is calculated with respect to a fatigue criterion. The assumption is made that the critical plane is the one where the variance of the equivalent stress is maximum.

The French method uses a multiaxial fatigue criterion that defines a damage indicator E_h for any physical plane. The crack initiation plane is assumed to be the critical plane, i.e. the fracture plane. The steps of the two procedures are detailed in the next sections.

The validation of the two methods against some experimental cyclic and random biaxial fatigue tests results is realized. The predicted crack initiation planes are compared with experimental ones. An extension of the two methods to multiaxial random stress states is then proposed. Tests carried out in the Polish laboratory allow to compare the assessed orientation of the fracture plane with the one observed on cruciform specimen submitted to biaxial random tensile-compressive loads.

Presentation of the variance method

Multiaxial stress states due to the action of various external loads exist at the considered point of the machine or structure. In the proposed algorithm the multiaxial stress states history is reduced to an uniaxial equivalent one by a maximum shear and normal stresses criterion (1). It is assumed that the fracture is influenced only by those stress components which act on the expected fracture plane(s). The generalized criterion is formulated as :

$$\max_t\left\{B\tau_{hs}(t)+K\sigma_h(t)\right\}=F \qquad (1)$$

where $\tau_{hs}(t)$ and $\sigma_h(t)$ are respectively shear stress in $\vec{s}$ direction and normal stress acting on the critical plane, which unit normal vector is denoted $\vec{h}$. The direction $\vec{s}$ agrees with the mean direction of the maximum shear stress $\tau_{hsmax}(t)$. $\tau_{hs}(t)$ and $\sigma_h(t)$ are functions of stress components $\sigma_{ij}(t)$ (i, j = x, y, z. B, K and F are constants of the criterion. K is expressed as :

$$K=\sqrt{\left(\frac{\sigma_{-1}}{2\tau_{-1}-\sigma_{-1}}\right)^2-1} \qquad (2)$$

where σ_{-1} and τ_{-1} are the material fatigue limits determined during completely reversed tensile and torsion tests respectively (R=-1).

In particular case of the criterion (B=1) the equivalent stress $\sigma_{eq}(t)$ is defined as :

$$\begin{aligned}\sigma_{eq}(t)=\frac{1}{1+K}\Big\{&\left[\hat{l}_1^2-\hat{l}_3^2+K\left(\hat{l}_1+\hat{l}_3\right)^2\right]\sigma_{xx}(t)+\left[\hat{m}_1^2-\hat{m}_3^2+K\left(\hat{m}_1+\hat{m}_3\right)^2\right]\sigma_{yy}(t)+\\&+\left[\hat{n}_1^2-\hat{n}_3^2+K\left(\hat{n}_1+\hat{n}_3\right)^2\right]\sigma_{zz}(t)+2\left[\hat{l}_1\hat{m}_1-\hat{l}_3\hat{m}_3+K\left(\hat{l}_1+\hat{l}_3\right)\left(\hat{m}_1+\hat{m}_3\right)\right]\sigma_{xy}(t)+\\&+2\left[\hat{l}_1\hat{n}_1-\hat{l}_3\hat{n}_3+K\left(\hat{l}_1+\hat{l}_3\right)\left(\hat{n}_1+\hat{n}_3\right)\right]\sigma_{xz}(t)+\\&+2\left[\hat{n}_1\hat{m}_1-\hat{n}_3\hat{m}_3+K\left(\hat{n}_1+\hat{n}_3\right)\left(\hat{m}_1+\hat{m}_3\right)\right]\sigma_{yz}(t)\Big\}\end{aligned} \qquad (3)$$

where $\hat{l}_n$, $\hat{m}_n$, $\hat{n}_n$ (n=1,2,3) are mean direction cosines of principal stresses written so that $\sigma_1(t)\geq\sigma_2(t)\geq\sigma_3(t)$. These direction cosines are used in the description of the expected fatigue fracture plane which is determined using direction cosines of its normal vector $\vec{h}$:

$$\hat{l}_h=\frac{\hat{l}_1+\hat{l}_3}{\sqrt{2}}; \qquad \hat{m}_h=\frac{\hat{m}_1+\hat{m}_3}{\sqrt{2}}; \qquad \hat{n}_h=\frac{\hat{n}_1+\hat{n}_3}{\sqrt{2}}. \qquad (4)$$

From equation (3) it appears that $\sigma_{eq}(t)$ is linearly depending on the stress state components $\sigma_{ij}(t)$. This can be simply written as :

$$\sigma_{eq}(t)=\sum_{k=1}^{6}a_kX_k(t) \qquad (5)$$

where : $X_1(t)=\sigma_{xx}(t)$, $X_2(t)=\sigma_{yy}(t)$, $X_3(t)=\sigma_{zz}(t)$,
$X_4(t)=\sigma_{xy}(t)$, $X_5(t)=\sigma_{xz}(t)$, $X_6(t)=\sigma_{yz}(t)$.

The variance of the equivalent stress can be calculated as :

$$\mu_{\sigma_{eq}}(t)=\sum_{s=1}^{6}\sum_{t=1}^{6}a_s a_t \mu_{xst} \tag{6}$$

where μ_{xst} are the components of the (6x6) covariance matrix of the variables X_k.

In general case the variance $\mu_{\sigma eq}$ depends on the direction cosines $\hat{l}_n$, $\hat{m}_n$, $\hat{n}_n$ (n=1,2,3) which have to fulfil 6 conditions of orthogonality. Practically, the direction cosines are expressed as functions of the three Type 1 Euler angles ψ, θ, φ (see figure 1)

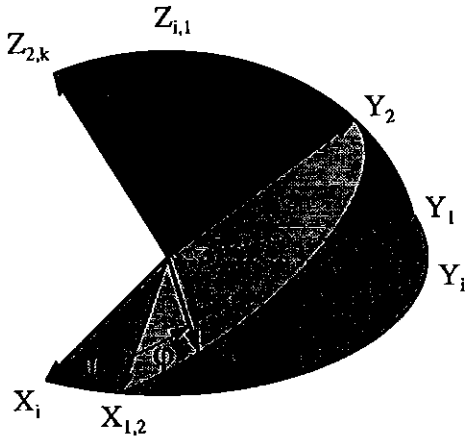

Fig. 1 Type 1 Euler angles.

By this way, the variance of the equivalent stress can be written as :

$$\mu_{\sigma_{eq}}=f(\psi,\theta,\varphi,K,\mu_{xst}) \tag{7}$$

As K and μ_{xst} are constants, $\mu_{\sigma eq}$ depends on the three parameters ψ, θ, φ. The determination of the maximum value of this function is generally not possible in an analytical way. Then it is numerically calculated.

In the case of multiaxial stationary and ergodic random stress history, the determination of the fracture plane is quite similar. The variance matrix is calculated from the representative parts of the stress histories and then the set of critical Euler angles (ψ_c, θ_c, φ_c) that gives the highest value to the variance of the equivalent stress is searched.

Presentation of the damage indicator method

Fracture plane assessment under cyclic stress states

The method which is developed in this section is a deterministic one with respect to the former. First, it is presented for a cyclic stress state $[\sigma(t)]$ that is known at the considered point M where the fatigue damage assessment is realized. The criterion defines a time dependent damage indicator $E_h(t)$ for any physical plane which unit normal vector is denoted $\vec{h}$. This damage indicator is a linear combination of the alternate shear stress $\tau_{ha}(t)$, the alternate normal stress $\sigma_{hha}(t)$ and the mean normal stress σ_{hhm} **(2)** as :

$$E_h(t) = \frac{1}{\theta(N)}\left[\tau_{ha}(t) + \alpha(N)\sigma_{hha}(t) + \beta(N)\sigma_{hhm}\right] \tag{8}$$

The damage indicator E_h corresponding to the physical plane is defined as the maximum value of $E_h(t)$ during the cycle.

$$E_h = \max_t\left[E_h(t)\right] \tag{9}$$

In this criterion, the normal and shear stress are distinguished as it is well recognized they do not have the same influence in fatigue. Concerning the normal stress, mean and alternate stresses are also separated because they do not have the same incidence on the fatigue behaviour of materials, as the tensile-compressive constant life diagram (Haigh diagram) demonstrates these differences of influence. The mean shear stress does not appear in the formulation of the damage indicator as it is generally assumed to have no practical influence on the fatigue behaviour.

The coefficients α and β describe the respective contribution of the stresses components to fatigue damage.

The critical plane (i.e. fracture plane) which unit normal vector is denoted $\vec{h}_c$ is the one for which the damage indicator is the highest .This maximum value is the fatigue function E of the criterion.

$$E = E_{h_c} = \max_{\vec{h}}\left[E_h\right] \tag{10}$$

E is generally used in order to check if a given multiaxial stress states cycle reaches the fatigue limit or the fatigue strengths (corresponding to N cycles) of the material. This is expressed as :

$$E = 1 \tag{11}$$

α, β and θ are the three parameters of the criterion. They are determined by stating that the criterion is checked (E=1) for the three fatigue limits of the material, or its three fatigue strengths corresponding to N cycles when the criterion is used as a N cycles fatigue criterion. In other words, it means that the criterion may be utilized as well for endurance limit as for finite fatigue lives **(2,3,4).**

A physical plane is determined by the two angles γ and φ as shown on figure 2. All the possible physical planes of the material are reviewed.

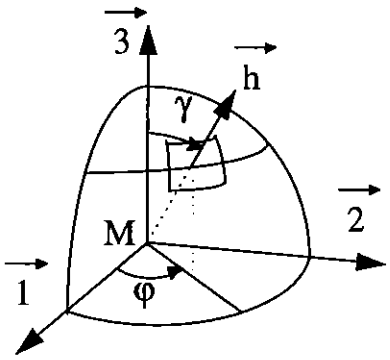

Fig. 2 Location of a physical plane.

The alternate normal stress $\sigma_{hha}(t)$ is calculated with :

$$\sigma_{hha}(t) = \sigma_{hh}(t) - \sigma_{hhm} \tag{12}$$

where σ_{hhm} is the mean value of $\sigma_{hh}(t)$ during the stress cycle :

$$\sigma_{hh}(t) = {}^{t}\{\vec{h}\}[\sigma(t)]\{\vec{h}\} \tag{13}$$

The alternate shear stress $\tau_{ha}(t)$ is defined by a geometrical method. During a cycle, the tip of the shear stress vector acting on the plane makes a closed loop. The smallest circle surrounding to this loop is built (figure 3).

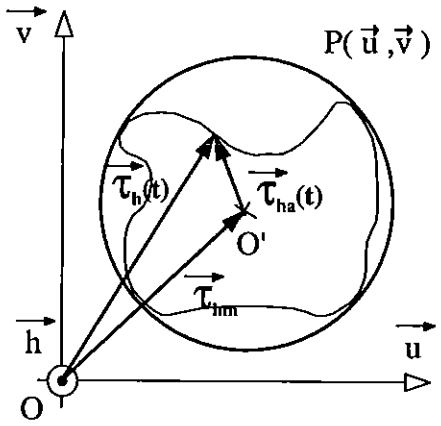

Fig. 3 Definition of the alternate shear stress vector $\vec{\tau}_{ha}(t)$.

The center of the circle gives the mean component $\vec{\tau}_{hm}$ of the shear stress vector $\vec{\tau}_h(t)$ during the cycle. The alternate shear stress vector $\vec{\tau}_{ha}(t)$ is obtained by :

$$\vec{\tau}_{ha}(t) = \vec{\tau}_h(t) - \vec{\tau}_{hm} \tag{13}$$

Fracture plane assessment under multiaxial random loading

The concept of a plane by plane damage cumulation is used for this purpose. The multiaxial random stress states history is decomposed into cycles by the way of the definition of a counting variable and the application of the Rainflow counting procedure to this variable. The normal stress acting on a physical plane is used as the counting variable (3). A multiaxial cycle is identified and extracted from the multiaxial stress history when a cycle of the counting variable is obtained from the corresponding part of the multiaxial history.

The criterion allows to calculate the life of the material through equation (10), plane after plane as shear and normal components of stresses are known for any plane. A damage law such as Miner's rule allows to determine the corresponding damage induced by the multiaxial cycle on that plane. The calculations are made for all the possible physical planes and for all the stress cycles. A damage cumulation is performed plane by plane for the whole multiaxial sequence (4). Finally, the most damaged plane is assumed to be the critical one, i.e. the fracture plane.

Comparison of both methods against experimental results

An experimental verification is realized in order to validate the methods. It is based on the results obtained from fatigue tests of specimens under biaxial cyclic and random states of stress. They are issued from experiments found in literature connected with fatigue fracture planes. Collected tests results are those for which fatigue material data are complete - that is necessary for the application of the two methods - and fracture planes orientations are precisely described.

Cyclic biaxial stress states tests

Six sets of experimental results (corresponding to 86 tests) were collected and are given in table 1. Rotvel (5) made his experiments with cylindrical 0.35% carbon steel specimens. Biaxial sinusoidal tension-compression stress states were generated with different values of mean stress and for some cases out of phase. Nishihara and Kawamoto (6) obtained the orientation of the fracture planes under complex bending and torsion cyclic tests. Various ratios of stress amplitudes and many different dephasings are provided. Round specimens were used and several materials are investigated : 0.51% carbon hardened steel, 0.1% carbon mild steel, 3.87% carbon cast iron and 3.81% Cu duraluminium. Achtelik et al. (7) tested grey cast iron Zl 250 (3.32% C) round specimens under bending-torsion stress states.

Table 1. Cyclic stress states and fatigue data

Material : carbon steel 0.35% C, σ_{-1}=215.8 MPa, σ_0=349.9 MPa, τ_{-1}=138.5 MPa, Rm=570 MPa (5)

Test number	Stress states	
	$\sigma_{xx}(t)$	$\sigma_{yy}(t)$
1	227.6 sin(ωt)	1.96 sin(ωt)
2	-2.94 + 224.6 sin(ωt)	6.87 sin(ωt + π)
3	52 + 233.5 sin(ωt)	41.2 + 191.3 sin(ωt)
4	-11.8 + 228.6 sin(ωt)	-24.5 + 117.7 sin(ωt)
5	-7.8 + 156 sin(ωt)	11.77 + 121.6 sin(ωt + π)
6	79.5 + 155 sin(ωt + π)	118.7 sin(ωt)

Material : hardened steel 0.51% C, σ_{-1}=313.9 MPa, σ_0=485.8 MPa, τ_{-1}=196.2 MPa, Rm=694 MPa (6)

Test number	Stress states	
	$\sigma_{xx}(t)$	$\sigma_{xy}(t)$
HNK50	0.0	225.63 sin(ωt)
HNK53	353.16 sin(ωt)	0.0
HNK54	0.0	201.11 sin(ωt)
HNK55	323.73 sin(ωt)	0.0
HNK59	294.30 sin(ωt + π/2)	147.15 sin(ωt)
HNK60	274.68 sin(ωt)	137.34 sin(ωt)
HNK63	264.87 sin(ωt + π/2)	132.44 sin(ωt)
HNK67	162.85 sin(ωt + π/2)	196.69 sin(ωt)
HNK69	154.45 sin(ωt + π/2)	184.23 sin(ωt)
HNK74	162.85 sin(ωt)	195.69 sin(ωt)
HNK75	308.03 sin(ωt)	63.86 sin(ωt)
HNK76	141.85 sin(ωt)	171.28 sin(ωt)

Material : hardened steel 0.51% C, σ_{-1}=313.9 MPa, σ_0=485.8 MPa, τ_{-1}=196.2 MPa, Rm=694 MPa (6)

Test number	Stress states	
	$\sigma_{xx}(t)$	$\sigma_{xy}(t)$
HNK79	344.33 sin(ωt)	71.32 sin(ωt)
HNK83	344.33 sin(ωt + π/2)	71.32 sin(ωt)
HNK84	157.65 sin(ωt + π/3)	190.31 sin(ωt)
HNK86	308.03 sin(ωt + π/3)	63.86 sin(ωt)
HNK89	255.06 sin(ωt)	127.53 sin(ωt)
HNK90	264.87 sin(ωt + π/3)	132.44 sin(ωt)
HNK91	255.06 sin(ωt + π/3)	127.53 sin(ωt)
HNK94	147.15 sin(ωt + π/3)	177.56 sin(ωt)
HNK96	141.95 sin(ωt + π/6)	171.18 sin(ωt)
HNK97	152.35 sin(ωt + π/6)	183.94 sin(ωt)
HNK98	264.87 sin(ωt + π/6)	132.44 sin(ωt)
HNK99	255.06 sin(ωt + π/6)	127.53 sin(ωt)

Material : soft steel 0.1% C, σ_{-1}=235.4 MPa, σ_0=325.7 MPa, τ_{-1}=137.3 MPa, Rm=382 MPa (6)

Test number	Stress states	
	$\sigma_{xx}(t)$	$\sigma_{xy}(t)$
LNK5	194.30 sin(ωt)	0.0
LNK11	0.0	142.25 sin(ωt)
LNK12	187.12 sin(ωt)	93.59 sin(ωt)
LNK16	101.34 sin(ωt)	122.33 sin(ωt)
LNK18	235.64 sin(ωt)	48.85 sin(ωt)
LNK22	235.83 sin(ωt + π/2)	117.92 sin(ωt)
LNK24	208.07 sin(ωt + π/2)	104.08 sin(ωt)
LNK27	112.62 sin(ωt + π/2)	135.97 sin(ωt)
LNK28	244.76 sin(ωt + π/2)	50.72 sin(ωt)
LNK29	235.64 sin(ωt + π/2)	48.85 sin(ωt)
LNK31	201.11 sin(ωt + π/3)	100.55 sin(ωt)
LNK32	194.24 sin(ωt + π/3)	97.12 sin(ωt)
LNK35	245.25 sin(ωt)	0.0
LNK36	105.16 sin(ωt + π/3)	126.84 sin(ωt)
LNK40	108.89 sin(ωt + π/3)	131.45 sin(ωt)

Material : cast iron 3.87% C, σ_{-1}=96.1 MPa, σ_0=142.3 MPa, τ_{-1}=91.2 MPa, Rm=185 MPa (6)

Test number	Stress states	
	$\sigma_{xx}(t)$	$\sigma_{xy}(t)$
CNK4	103.0 sin(ωt)	0.0
CNK6	96.19 sin(ωt)	0.0
CNK7	83.38 sin(ωt)	41.59 sin(ωt)
CNK12	95.16 sin(ωt)	19.72 sin(ωt)
CNK16	104.18 sin(ωt + π/2)	21.58 sin(ωt)
CNK19	99.57 sin(ωt + π/2)	20.6 sin(ωt)
CNK23	56.31 sin(ωt)	67.98 sin(ωt)
CNK30	93.68 sin(ωt + π/3)	46.89 sin(ωt)
CNK33	67.59 sin(ωt + π/3)	81.62 sin(ωt)

Material : cast iron 3.87% C, σ_{-1}=96.1 MPa, σ_0=142.3 MPa, τ_{-1}=91.2 MPa, Rm=185 MPa (6)

Test number	Stress states	
	$\sigma_{xx}(t)$	$\sigma_{xy}(t)$
CNK36	0.0	98.1 sin(ωt)
CNK38	75.05 sin(ωt + π/2)	90.64 sin(ωt)
CNK39	71.32 sin(ωt + π/2)	86.13 sin(ωt)

Material : duraluminium 3.81% Cu, σ_{-1}=156 MPa, σ_0=257.1 MPa, τ_{-1}=100 MPa, Rm=443 MPa (6)

Test number	Stress sates	
	$\sigma_{xx}(t)$	$\sigma_{xy}(t)$
D-30 2	0.0	98.1 sin(ωt)
D-30 5	0.0	127.53 sin(ωt)
D-30 6	156.96 sin(ωt)	0.0
D-30 7	196.2 sin(ωt + π/2)	0.0
D-30 8	181.29 sin(ωt + π/2)	37.57 sin(ωt)
D-30 12	152.55 sin(ωt)	76.32 sin(ωt)
D-30 15	138.7 sin(ωt + π/2)	69.36 sin(ωt)
D-30 16	124.88 sin(ωt)	62.49 sin(ωt)
D-30 17	163.14 sin(ωt)	33.75 sin(ωt)
D-30 19	117.92 sin(ωt + π/2)	58.96 sin(ωt)
D-30 20	82.6 sin(ωt)	99.67 sin(ωt)
D-30 22	199.44 sin(ωt)	41.3 sin(ωt)
D-30 23	199.44 sin(ωt + π/2)	41.3 sin(ωt)
D-30 24	82.6 sin(ωt + π/2)	99.67 sin(ωt)

Material : grey cast iron 3.32% Cu, σ_{-1}=143 MPa, σ_0=212.7 MPa, τ_{-1}=110 MPa, Rm=278.8 MPa (7)

Test number	Stress states	
	$\sigma_{xx}(t)$	$\sigma_{xy}(t)$
Zla 1	168.0 sin(ωt)	0.0
Zla 2	164.0 sin(ωt)	0.0
Zla 3	160.0 sin(ωt)	0.0
Zlb 1	0.0	142.0 sin(ωt)
Zlb 2	0.0	130.0 sin(ωt)
Zlb 3	0.0	132.0 sin(ωt)
Zlc 1	149.9 sin(ωt)	74.95 sin(ωt)
Zlc 2	121.62 sin(ωt)	60.81 sin(ωt)
Zlc 3	118.79 sin(ωt)	59.4 sin(ωt)
Zld 1	176.67 sin(ωt)	51.0 sin(ωt)
Zld 2	155.88 sin(ωt)	45.0 sin(ωt)
Zld 3	152.42 sin(ωt)	44.0 sin(ωt)
Zle 1	118.0 sin(ωt)	102.2 sin(ωt)
Zle 2	108.0 sin(ωt)	93.53 sin(ωt)
Zle 3	106.0 sin(ωt)	91.78 sin(ωt)

Random biaxial stress state tests

Some biaxial random tension-compression fatigue tests have been carried out in the Technical University of Opole (Poland) by W. Będkowski (8) and E. Macha. Low carbon steel (10 HNAP) thin walled cruciform specimens were used. The table 2 gives the chemical composition of this steel. Ten different random sequences were generated by a random signals generator. The track of the fracture plane with the (O, x, y) free surface plane was observed through angle α_r as shown on figure 4. The unit vector $\vec{h}_r$ normal to this fracture plane is such that : $(\vec{h}_r, \vec{x}) = \alpha_r \pm 90°$.

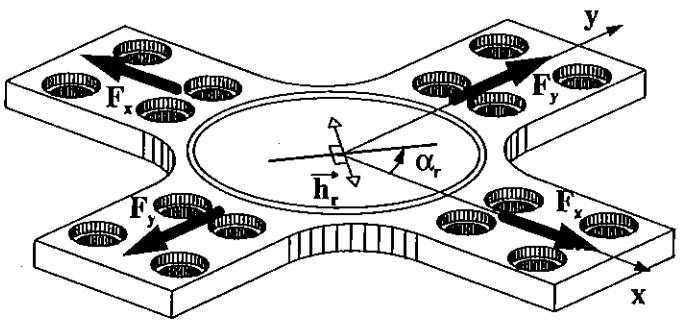

Fig. 4 Cruciform specimen description.

Table 2. Chemical composition of the 10 HNAP steel.

Elements	C	Mn	Si	P	S	Cr	Cu	Ni
Content [%]	0.115	0.71	0.41	0.082	0.028	0.81	0.30	0.50

Fracture plane orientation results

The experimental fracture plane is defined by its unit normal vector $\vec{h}_r$. Predicted fracture planes are defined by the theoretical unit normal vector $\vec{h}_{t1}$ and $\vec{h}_{t2}$ for variance and damage indicator methods respectively. In the case where several assessed fracture plane are obtained, the most similar to that obtained experimentally is assumed. The suitability of the predicting methods is measured by the closeness of the theoretical and experimentally observed fracture planes, it is to say by the closeness of the corresponding unit normal vectors $\vec{h}_r$ and $\vec{h}_{t1,t2}$. The dot product of these vectors is calculated to express the agreement (or disagrement) between assessments and tests results.

The direction cosines of vectors $\vec{h}_r$, $\vec{h}_{t1}$ and $\vec{h}_{t2}$ are reported in table 3 for biaxial cyclic tests and in table 4 for biaxial random tests.

Table 3. Experimental and predicted fracture plane orientations (cyclic stress states)

Test number	real cosines directions			theoretical variance cosines directions				theoretical damage indicator cosines directions			
	l_r	m_r	n_r	l_{t1}	m_{t1}	n_{t1}	$\vec{h}_r \cdot \vec{h}_{t1}$	l_{t2}	m_{t2}	n_{t2}	$\vec{h}_r \cdot \vec{h}_{t2}$
1	1.0	0.0	0.0	0.990	0.143	0.0	0.990	0.845	0.074	-0.530	0.845
2	1.0	0.0	0.0	0.990	0.143	0.0	0.990	0.842	0.526	0.122	0.842
3	1.0	0.0	0.0	0.990	0.143	0.0	0.990	0.848	0.0	-0.530	0.848
4	1.0	0.0	0.0	0.990	0.143	0.0	0.990	0.839	0.0	-0.545	0.839
5	1.0	0.0	0.0	0.990	0.143	0.0	0.990	0.829	0.559	0.0	0.829
6	1.0	0.0	0.0	0.990	0.143	0.0	0.990	0.848	0.530	0.0	0.848
HNK50	0.71	0.71	0.0	0.791	0.612	0.0	0.996	0.982	0.191	0.0	0.832
HNK53	1.0	0.0	0.0	0.992	0.126	0.0	0.992	0.833	-0.337	0.438	0.833
HNK54	0.71	0.71	0.0	0.791	0.791	0.0	0.996	0.982	0.191	0.0	0.832
HNK55	1.0	0.0	0.0	0.992	0.126	0.0	0.992	0.835	0.543	0.087	0.835
HNK59	1.0	0.0	0.0	0.992	0.124	0.0	0.992	0.875	-0.485	0.0	0.875
HNK60	0.92	0.38	0.0	0.965	0.264	0.0	0.988	0.978	-0.208	0.0	0.821
HNK63	1.0	0.0	0.0	0.992	0.124	0.0	0.992	0.876	-0.466	0.122	0.876
HNK67	0.91	0.41	0.0	0.848	0.530	0.0	0.990	0.988	0.156	0.0	0.963
HNK69	0.88	0.47	0.0	0.848	0.53	0.0	0.995	0.985	0.174	0.0	0.948

HNK74	0.82	0.57	0.0	0.755	0.655	0.0	0.992	0.375	0.927	0.0	0.836
HNK75	0.98	0.19	0.0	0.998	0.069	0.0	0.991	0.927	-0.375	0.0	0.837
HNK76	0.83	0.56	0.0	0.755	0.655	0.0	0.993	0.375	0.927	0.0	0.830
HNK79	0.98	0.19	0.0	0.998	0.069	0.0	0.991	0.927	-0.374	0.035	0.837
HNK83	1.0	0.0	0.0	0.992	0.126	0.0	0.992	0.837	0.483	0.259	0.837
HNK84	0.92	0.39	0.0	0.881	0.473	0.0	0.995	0.999	0.052	0.0	0.939
HNK86	1.0	0.0	0.0	0.992	0.126	0.0	0.992	0.837	0.483	0.259	0.837
HNK89	0.93	0.37	0.0	0.965	0.264	0.0	0.995	0.982	0.191	0.0	0.843
HNK90	0.99	0.14	0.0	0.983	0.181	0.0	0.999	0.978	-0.208	0.0	0.939
HNK91	0.99	0.14	0.0	0.983	0.181	0.0	0.999	0.978	0.-208	0.0	0.939
HNK94	0.93	0.37	0.0	0.881	0.473	0.0	0.994	0.999	0.053	0.0	0.948
HNK96	0.85	0.53	0.0	0.892	0.452	0.0	0.998	1.0	0.0	0.0	0.850
HNK97	0.92	0.39	0.0	0.892	0.452	0.0	0.997	1.0	0.0	0.0	0.920
HNK98	0.96	0.28	0.0	0.968	0.251	0.0	1.0	0.978	-0.208	0.0	0.881
HNK99	0.96	0.28	0.0	0.968	0.251	0.0	1.0	0.978	-0.208	0.0	0.881
LNK5	1.0	0.0	0.0	0.997	0.077	0.0	0.997	0.810	0.487	0.326	0.810
LNK11	0.71	0.71	0.0	0.764	0.645	0.0	0.996	0.990	0.139	0.0	0.802
LNK12	0.93	0.37	0.0	0.953	0.303	0.0	0.998	0.970	-0.242	0.0	0.813
LNK16	0.87	0.49	0.0	0.874	0.486	0.0	0.999	0.999	-0.052	0.0	0.843

Test number	real cosines directions			theoretical variance cosines directions				theoretical damage indicator cosines directions			
	l_r	m_r	n_r	l_{t1}	m_{t1}	n_{t1}	$\vec{h}_r \cdot \vec{h}_{t1}$	l_{t2}	m_{t2}	n_{t2}	$\vec{h}_r \cdot \vec{h}_{t2}$
LNK18	0.98	0.20	0.0	0.961	0.276	0.0	0.997	0.680	0.730	0.07	0.813
LNK22	0.99	0.14	0.0	0.997	0.077	0.0	0.998	0.875	0.485	0.0	0.934
LNK24	0.99	0.14	0.0	0.997	0.077	0.0	0.998	0.875	0.485	0.0	0.934
LNK27	0.78	0.63	0.0	0.826	0.564	0.0	0.999	0.999	0.139	0.0	0.860
LNK28	1.0	0.0	0.0	0.997	0.077	0.0	0.997	0.810	0.487	0.326	0.810
LNK29	1.0	0.0	0.0	0.997	0.077	0.0	0.997	0.810	0.487	0.326	0.810
LNK31	0.99	0.14	0.0	0.975	0.222	0.0	0.996	0.970	-0.242	0.0	0.927
LNK32	0.98	0.20	0.0	0.975	0.222	0.0	1.0	0.970	-0.242	0.0	0.903
LNK35	1.0	0.0	0.0	0.997	0.077	0.0	0.997	0.810	0.487	0.326	0.810
LNK36	0.93	0.37	0.0	0.861	0.509	0.0	0.989	0.999	0.017	0.0	0.936
LNK40	0.99	0.14	0.0	0.860	0.512	0.0	0.923	0.999	0.017	0.0	0.992
CNK4	1.0	0.0	0.0	0.848	0.530	0.0	0.848	0.991	-0.052	-0.122	0.991
CNK6	1.0	0.0	0.0	0.848	0.530	0.0	0.848	0.991	-0.052	-0.122	0.991
CNK7	0.91	0.41	0.0	0.986	-0.166	0.0	0.848	0.865	0.499	-0.052	0.992
CNK12	0.98	0.20	0.0	0.729	0.684	0.0	0.851	0.946	0.326	0.0	0.992
CNK16	1.0	0.0	0.0	0.848	0.530	0.0	0.848	0.991	-0.052	-0.122	0.911
CNK19	1.0	0.0	0.0	0.848	0.530	0.0	0.848	0.991	-0.052	-0.122	0.911

CNK23	0.83	0.56	0.0	0.999	0.032	0.0	0.867	0.731	0.682	0.0	0.989
CNK30	0.96	0.28	0.0	0.976	-0.216	0.0	0.876	0.982	0.191	0.0	0.996
CNK33	0.84	0.54	0.0	0.996	0.087	0.0	0.887	0.891	0.454	0.0	0.994
CNK36	0.71	0.71	0.0	0.974	0.226	0.0	0.857	0.809	0.588	0.0	0.992
CNK38	0.79	0.61	0.0	0.983	0.183	0.0	0.888	0.857	0.515	0.0	0.991
CNK39	0.80	0.60	0.0	0.983	0.183	0.0	0.896	0.857	0.515	0.0	0.995
D-30 2	1.0	0.0	0.0	0.801	-0.598	0.0	0.801	0.996	0.087	0.0	0.996
D-30 5	1.0	0.0	0.0	0.801	-0.598	0.0	0.801	0.996	0.087	0.0	0.996
D-30 6	0.97	0.24	0.0	0.990	0.141	0.0	0.994	0.846	0.529	0.070	0.947
D-30 7	0.98	0.20	0.0	0.990	0.141	0.0	0.998	0.846	0.529	0.070	0.935
D-30 8	0.88	0.47	0.0	0.999	0.045	0.0	0.900	0.896	0.545	0.0	0.994
D-30 12	0.87	0.49	0.0	0.86	0.510	0.0	0.998	0.574	0.819	0.0	0.900
D-30 15	1.0	0.0	0.0	0.990	0.141	0.0	0.990	0.882	-0.469	0.052	0.882
D-30 16	0.82	0.57	0.0	0.860	0.510	0.0	0.996	0.574	0.819	0.0	0.937
D-30 17	0.80	0.60	0.0	0.943	0.334	0.0	0.995	0.719	0.695	0.0	0.992
D-30 19	1.0	0.0	0.0	0.990	0.141	0.0	0.990	0.882	-0.469	0.052	0.882
D-30 20	1.0	0.0	0.0	0.903	0.429	0.0	0.903	1.0	0.0	0.0	1.0
D-30 22	0.82	0.57	0.0	0.943	0.334	0.0	0.964	0.719	0.695	0.0	0.986
D-30 23	0.85	0.53	0.0	0.990	0.045	0.0	0.873	0.839	0.545	0.0	1.0
D-30 24	1.0	0.0	0.0	0.857	-0.515	0.0	0.857	0.999	-0.052	0.0	0.999
Zla 1	1.0	0.0	0.0	0.960	0.281	0.0	0.960	0.916	-0.370	0.156	0.916
Zla 2	1.0	0.0	0.0	0.960	0.281	0.0	0.960	0.916	-0.370	0.156	0.916
Zla 3	1.0	0.0	0.0	0.960	0.281	0.0	0.960	0.916	-0.370	0.156	0.916
Zlb 1	0.71	0.71	0.0	0.878	0.479	0.0	0.963	0.342	0.940	0.0	0.910
Zlb 2	0.71	0.71	0.0	0.878	0.479	0.0	0.963	0.342	0.940	0.0	0.910
Zlb 3	0.71	0.71	0.0	0.878	0.479	0.0	0.963	0.342	0.940	0.0	0.910
Zlc 1	0.88	0.47	0.0	0.779	0.627	0.0	0.980	0.682	0.731	0.0	0.944
Zlc 2	0.88	0.47	0.0	0.779	0.627	0.0	0.980	0.682	0.731	0.0	0.944
Zlc 3	0.91	0.42	0.0	0.994	0.108	0.0	0.950	0.682	0.731	0.0	0.928
Zld 1	0.95	0.30	0.0	0.854	0.520	0.0	0.967	0.777	0.629	0.0	0.927
Zld 2	0.96	0.29	0.0	0.854	0.520	0.0	0.971	0.777	0.629	0.0	0.929
Zld 3	0.97	0.23	0.0	1.0	0.0	0.0	0.970	0.988	-0.156	0.0	0.922
Zle 1	0.81	0.59	0.0	0.690	0.724	0.0	0.986	0.574	0.819	0.0	0.948
Zle 2	0.80	0.60	0.0	0.690	0.724	0.0	0.986	0.574	0.819	0.0	0.950
Zle 3	0.82	0.57	0.0	0.690	0.724	0.0	0.978	0.574	0.819	0.0	0.937

Table 4. Experimental and predicted fracture plane orientations (random stress states)

Sequences	Experimental fracture plane angle α_r (degrees)	Theoretical variance method angle α_{t1} (degrees)	Theoretical damage indicator method angle α_{t2} (degrees)
GP9302	72.0	71.2	30.0 (60.0)
	-73.5	-73.0	-30.0(-60.0)
	-11.0		
GP9305	-62.0	-71.9	30.0 (60.0)
		72.3	-30.0 (-60.0)
GP9307	-73.5	-73.6	30.0 (60.0)
	-67.0		-30.0 (-60.0)
GP9308	71.0	72.8	30.0 (60.0)
		-71.4	-30.0 (-60.0)
GP9310	-25.0	-17.9	-30.0
		17.9	30.0
GP9312	-72.5	-72.8	-60.0
		71.4	60.0
GP9313	-71.0	-75.4	-60.0
		68.7	60.0
GP9314	-70.0	-73.5	-60.0
		70.6	60.0
GP9315	68.0	70.0	65.0
	-70.5	-74.2	-65.0
GP9619	-65.0	-69.7	-65.0
	-42.0	74.5	65.0

Discussion

In the case of cyclic stress states tests, the variance method gives very good prediction of the fracture plane orientation. It provides the best predictions for the tests carried on 0.35% C steel, 0.51% C hardened steel, 0.1% C soft steel, grey cast iron (3.32% Cu). The damage indicator (deterministic) method gives the most suitable predicted results for the cast iron (3.87% C) and the two assessing methods are equivalent for the duraluminium.

The overall mean value of the dot product is about 0.961 for the variance method and 0.908 for the deterministic one. It indicates an average deviation angles of 16.1° and 24.7° respectively of the predicted fracture planes against the real ones.

Possible explanations of the deviation between predicted and experimental fracture planes may be caused by heterogeneous defaults of metals which become crack initiation sites because of local stress concentrations and / or mechanical weakness of the material.

Such defects are responsible of modification of the crack initiation plane direction because of local changes of stress states. The second explanation is an average effect. In the case of many equally critical planes each one quite close from each other, the macroscopic fracture plane can be observed as the average fracture plane. The figure 5 shows for instance the distribution of the damage indicator all over the possible material planes (which unit normal vector is defined with angles φ and γ) for a non proportional bending-torsion cyclic fatigue test. All the critical planes make a ring and because of many activated slipping planes, the real fracture plane has a unit normal vector close to the average of the set of unit vectors of all the critical planes.

This phenomenon is presented on the figure 5 for the damage indicator method. It is also available for the statistical variance method.

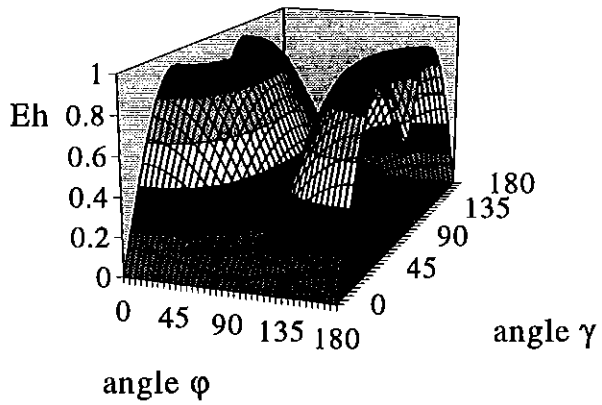

Fig. 5 Distribution of the damage indicator.

In the case of biaxial random stress histories, the mean angle deviation between predicted and experimental fracture planes are closed to 3.3° for the variance method and 20.0° for the damage indicator method if only the most critical plane is considered. For this method some other critical fracture planes may appear and are reported mentioned between brackets in table 4. They correspond to other critical plane (figure 6), even if the cumulated damage D_h is less than the one obtained on the principal damaged planes. When these planes are also considered the mean deviation between predictions and experiments is represented by a 7.4° angle.

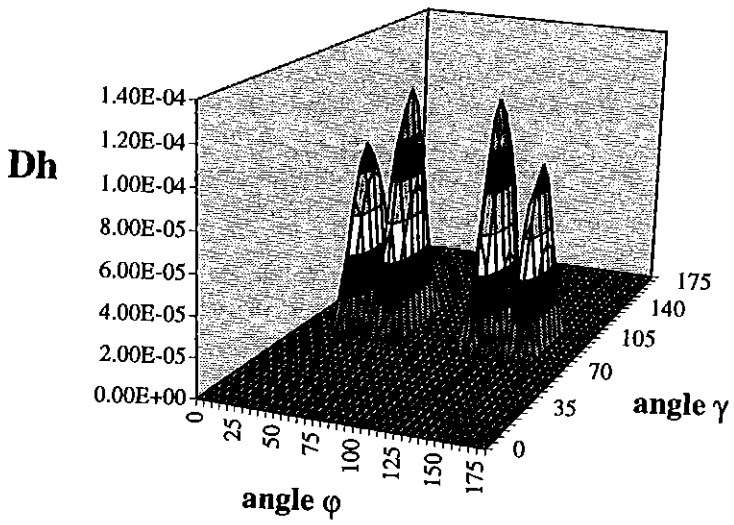

Fig. 6 Plane by plane cumulated damage.

Conclusion

Two statistical and deterministic methods for predicting fracture plane orientation have been described and compared against experimental results concerning cyclic and random biaxial stress states. The statistical approach uses the variance of an equivalent stress which is a linear combination of the normal and shear stresses acting on a plane. It is assumed that the fracture plane is the one where the variance of the equivalent stress is the highest. The deterministic method uses a critical plane criterion that defines a damage indicator for any physical plane. It is a function of the alternate and mean components of the normal and shear stresses acting on this plane. The fracture plane corresponds to the most damaged one.

In the case of low mean stress the variance approach is a very promising method for the fracture plane assessment.

As a matter of fact, this stage is a preliminary step for fatigue life assessment. The accuracy of the fatigue life prediction methods strongly depends on the ability to determine the critical plane of the material as the crack initiation is directly related to this plane.

References

(1) BĘDKOWSKI W., MACHA E., (1992), Fatigue fracture plane under multiaxial random loadings - Prediction by variance of equivalent stress based on the maximum shear and normal stresses, Mat.-wiss. u. Werkstofftech. 23, pp.82-94

(2) ROBERT J.L., (1992), Contribution à l'étude de la fatigue multiaxiale sous sollicitations périodiques ou aléatoires, Thesis of the National Institute of Applied Sciences (INSA) of Lyon. Order number 92ISAL0004

(3) KENMEUGNE B., (1996), Contribution à la modélisation du comportement en fatigue sous sollicitations multiaxiales d'amplitude variable, Thesis of the National Institute of Applied Sciences (INSA) of Lyon, Order number 96ISAL0064

(4) WEBER B., CLEMENT J.C., KENMEUGNE B., ROBERT J.L., (1997), On a global stress-based approach for fatigue assessment under multiaxial random loading, Engineering Against Fatigue, Sheffield

(5) ROTVEL F., (1970), Biaxial fatigue tests with zero mean stresses using tubular specimens, Int. J. of Mech. Sc., Pergamon Press, vol. 12, pp.597-615

(6) NISHIHARA T., KAWAMOTO M., (1945), The strength of metals under combined alternating bending and torsion with phase difference, Memoirs of the College of Engineering, Kyoto Imperial University, vol. XI, n°4, pp.95-112

(7) ACHTELIK H., JAKUBOWSKA I., MACHA E, (1983), Actual and estimated directions of fatigue fracture plane in ZI250 grey cast iron under combined alternating bending and torsion, Studia Geotechnica et Mechanica, vol. V, n°2, pp.9-30

(8) BĘDKOWSKI W., (1994), Determination of the critical plane and effort criterion in fatigue life evaluation for materials under multiaxial random loading - Experimental verification based on fatigue tests of cruciform specimens, Sixth International Spring Meeting - Fourth International Conference on Biaxial / Multiaxial F atigue, SF2M, Paris, pp.435-447